e-ISSN: 2550-164X

Available online at
https://jmeche.uitm.edu.my/browse-journals/regular-issue/regular-issue-2025-vol-22-3/

Journal of Mechanical Engineering 22(3) 2025, 120 – 136.

Journal of Mechanical Engineering

The Performance of Solar PVT Cooling through Hybrid Alumina-Silica Nanofluids in Water

Nur Hanani Mohd Radzuan[1], Irnie Azlin Zakaria[1,2,3*], Nor Afifah Yahaya[1], Nurlisa Hamzan[1], Anwar Ilmar Ramadhan[4]

[1]*Faculty of Mechanical Engineering, Universiti Teknologi MARA (UiTM), Shah Alam, Selangor, Malaysia.*
[2]*Energy Efficient Conversion Technology (EECT),Universiti Teknologi MARA (UiTM), Shah Alam, Selangor, Malaysia.*
[3]*Solar Research Institute (SRI), Universiti Teknologi MARA (UiTM), Shah Alam, Selangor, Malaysia.*
[4]*Department of Mechanical Engineering, Faculty of Engineering, Universitas Muhammadiyah Jakarta, Indonesia.*

ARTICLE INFO

Article history:
Received 20 March 2025
Revised 23 May 2025
Accepted 4 July 2025
Online first
Published 15 September 2025

Keywords:
ANSYS fluent
Solar cooling
Serpentine flow
Hybrid nanofluids

DOI:
https://doi.org/10.24191/jmeche.v22i3.5754

ABSTRACT

The increased demand for efficient renewable solar energy has presented a substantial thermal management challenge for solar photovoltaic thermal (PVT) panels. Since temperature variations majorly affect solar panel efficiency, alternative choices for advanced cooling systems are desperately needed to guarantee better performance. Nanofluids are nanosized particles dispersed in a base fluid that has superior thermal conductivity properties to increase heat transfer performance. This research investigates the effect of an alumina-silica (Al_2O_3:SiO_2) hybrid nanofluid with a volume concentration of 0.5% in water as an alternative coolant in a serpentine channel. The study investigated three various mixing ratios, ranging from 10:90, 50:50, to 30:70 (Al_2O_3:SiO_2) in water with velocity inlet variations (0.0272 – 0.1360 m/s) upon application of 1000 W/m2 heat flux, to mimic the actual implementation of solar PVT. The impact of these hybrid nanofluids on heat transfer performance and pressure drop effect was investigated using computational fluid dynamics (CFD) simulations with Ansys Fluent software. The solar PVT panel temperature was reduced with the adoption of hybrid nanofluids by 0.2% to 0.3% as compared to the base fluid. The heat transfer increment for the 10:90 ratio is 10.2% and 16.9% as the flow rate increases. However, the pressure drop increased in the range of 9.36 Pa to 88.43 Pa and 11.37 Pa to 101.57 Pa for 10:90 and 30:70 respectively as compared to the base fluid. Therefore, hybrid nanofluids feasibility as a cooling fluid for solar PV panel thermal management need to be further reviewed.

[1*] Corresponding author. *E-mail address*: irnieazlin@uitm.edu.my
https://doi.org/10.24191/jmeche.v22i3.5754

INTRODUCTION

Renewable energy is becoming more widely used as an alternative energy source. The apparent disadvantages of fossil fuels, including environmental pollution and limited availability, have led many countries to prioritize the development of technology to harness renewable energy (Hussien et al., 2023; Praveenkumar et al., 2023), (Zakaria et al., 2014). Alternatively, solar energy is an emerging renewable power source due to its abundant availability, as it converts sunlight into usable electrical energy via solar panels (Nabi et al., 2023). Solar photovoltaic–thermal (PVT) harnesses both electrical and thermal energy from solar PV. The output of solar PVT is both electrical power and the heat recovered from cooling the solar PVT.

The thermal management of a solar panel is a crucial operating feature that is constantly improving through advanced coolants and novel cooling plate designs. Excessive heat on the solar cell causes overheating, significantly reducing electrical efficiency. At ambient temperatures of 25 °C, solar panels absorb around 80% of sunlight as heat. Only 20% is turned into electricity. Every 1 °C increase in solar cell temperature will reduce the solar panel efficiency by 0.5% (Salehi et al., 2023). Therefore, a higher heat dissipation between the working fluid and the solar panel's back surface is currently aggressively explored to reach a lower panel temperature. This reduction will lead to higher power output and improved thermal energy transmission (Akrouch et al., 2025; Hamzat et al., 2021). Among other initiatives used to improve the thermal management of solar PV are nanofluids as a cooling medium, phase change material adoption, and innovative designs of cooling channels (Ali et al., 2023).

Nanoparticles with their low specific heat capacity and superior thermal conductivity can rapidly transmit heat when suspended in a base fluid (Awais et al., 2021; Johari et al., 2022). A comprehensive thermophysical properties of Al_2O_3 and SiO_2 nanofluids was reported by (Khalid et al., 2019) (Zakaria et al., 2018). Sardarabadi & Passandideh-Fard (2016) have also conducted both simulation and experimental studies on the adoption of nanofluids of various metal oxides at 0.2% wt. to base fluid water in a photovoltaic thermal system (PVT). They observed a decrease in surface temperature of Al_2O_3, TiO_2, and ZnO nanofluids as compared to the base fluid of water. The temperature reduction has resulted in an increase in electrical efficiency of 6.4%, 6.46%, 6.36%, and 5.48%, respectively. This study showed that the concentration of nanoparticles affects efficiency, as an increasing concentration of nanoparticles (0.05 %wt - 10 %wt) has enhanced the thermal efficiency. An experimental result conducted by Salehi et al. (2023) indicated that the nanofluid with aluminum nanoparticles improved the solar panel efficiency and solar PV panel's output power by an average of 13.5% and 13.7%, respectively, compared to the base fluid. The experiment was assessed in Mashhad, Iran, on a sunny winter day in November 2020.

As an expansion of single nanofluids, hybrid nanofluids, which consist of multiple nanoparticles dispersed in a base fluid, have demonstrated enhanced thermal properties as compared to single nanofluids. This is due to the synergistic effects of the combination of nanoparticles used (Rostami et al., 2018). The study revealed that among effective combinations are Al_2O_3-SiO_2 hybrid nanofluids in PEMFC (Yatim et al., 2021). The same combination was also studied by Ali et al. (2023) and Salehi et al. (2023) on the heat sink for miniature channels, in which they examined the hydraulic and thermal characteristics of hybrid nanofluids of Al_2O_3 and SiO_2 in base fluid water. A similar hybrid combination was also studied by Khalid et al. (2021) and Preeti & Ojjela (2022), and they presented a superior cooling property compared to single and its base fluid. As mentioned by Preeti & Ojjela (2022), who observed an increase in Nusselt number up to 46% for a hybrid of SiO_2:Al_2O_3 (25%:75%) at a volume fraction of 0.2%. Kazemian et al. (2022) also explored other hybrid combinations, which were multiwall carbon nanotube-Al_2O_3, multiwall carbon nanotube-SiC, graphene:Al_2O_3, and (4) graphene-SiC in a novel combined photovoltaic/thermal and solar collector system. They conclude that the multiwall carbon nanotube-SiC hybrid nanofluid has the highest overall energy efficiency of 70.40% as compared to other fluids. Studies on solar PVT systems utilizing Al_2O_3 - CuO/water hybrid nanofluids have also been conducted by Ali et al. (2023).

https://doi.org/10.24191/jmeche.v22i3.5754

Apart from the nanofluids adoption as the cooling medium in solar PVT, the design of cooling plates is also studied for maximizing energy efficiency. Studies on solar PVT systems utilizing both mono and duo serpentine absorber channels (Ali et al., 2023) have reported that increasing the Reynolds number (Re) from 500 to 2000 improved the heat transfer coefficient convectively by 27 to 36% and 44 to 55% for the mono and duo serpentine channels, respectively. However, the pressure drop in the duo serpentine channel is worse than the mono serpentine channel, as it is increased by 10% and 29%, respectively. Alqatamin & Jinzhan (2025) have integrated a perforated V-shaped fin into the PVT system in the simulation work to achieve a 31.27 % reduction in solar cell temperature.

Studies on the mixture ratio variants in Al_2O_3:SiO_2 are still lacking. Vahidinia et al. (2021) studied Al_2O_3:SiO_2 in Syltherms 800, but only at 1.5 vol% concentration and 50:50 mixture ratio. Thus, this study is novel since it ranges across 3 mixture ratios. The study is also a continuity from the previous thermo-physical properties and thermal-electrical-hydraulic research of Al_2O_3:SiO_2 (Khalid et al., 2025; Khalid et al., 2021), which reported on the measured thermo-physical properties and is shown in the methodology section. This investigation covers a mixture ratio variation of hybrid Al_2O_3:SiO_2 studied before, which are 50:50, 30:70, and 10:90. These various mixture ratios of hybrid Al_2O_3:SiO_2 in water were simulated using ANSYS Fluent software in the photovoltaic thermal systems. The performances of these hybrid Al_2O_3:SiO_2 in terms of both heat transfer, pressure drop effect, and electric generation improvement were compared among all working fluids studied.

METHODOLOGY

Model Geometry

The PV panel, absorber, and cooling tubes are the three main components of a PVT cooling system model. For this simulation analysis, the model has been simplified to include only the PV panel and serpentine cooling tubes. The ANSYS Workbench software was used to create the models for simulation in ANSYS Fluent, as depicted in Fig 1. The geometry parameters for the model are shown in Table 1.

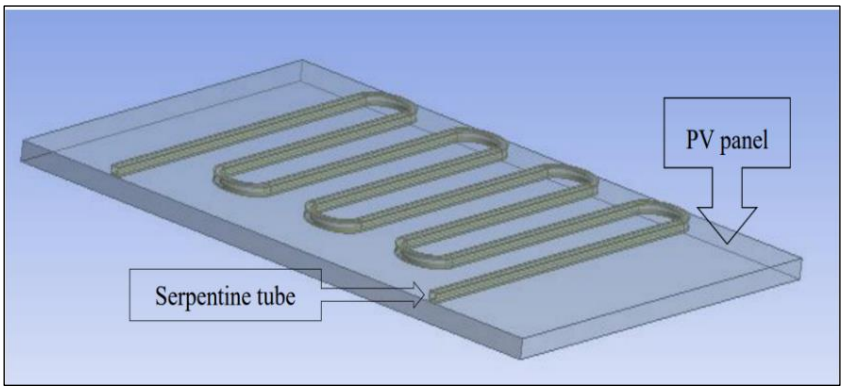

Fig. 1. Model of PVT plate.

Mesh Generation

The solar PVT system consists of two independent geometries: the solar panel's rectangular geometry and the pipe's square-shaped duct, which includes the fluid domain. A body-sizing method with an element size of 0.02 m was used for the solar PV panel body. The pipe and fluid domains with a square duct geometry were meshed using the multizone method, mainly using the hexahedral sweep type. The sweep

https://doi.org/10.24191/jmeche.v22i3.5754

method was used for tubes to create structured meshes in tube geometries. The edge sizing method is used at the tube geometry as it defines the number of divisions to improve the mesh resolution in important areas, ensuring the accurate representation of boundary layer effects and other specific phenomena. A layer of inflation was added to the tube, including 120 faces. As shown in Fig 2, the mesh generation generated three distinct domains: the solid domain, which models the PV panel and pipe, and the fluid domain, which models the flowing fluid inside the pipe and allows for the simulation of fluid flow and transmission of heat.

Table 1. Model parameters for the simulation (Price, 2025)

Component	Parameter	Value
PV panel	Material	Silicon
	Length	170 cm
	Width	100 cm
	Density	2329 kg/m^3
	Thermal conductivity	148 W/mK
Serpentine tube	Material	Copper
	Outer/ inner diameter	1.5 cm/ 1.25 cm
	Density	8987 kg/m^3
	Thermal conductivity	387.6 W/mK

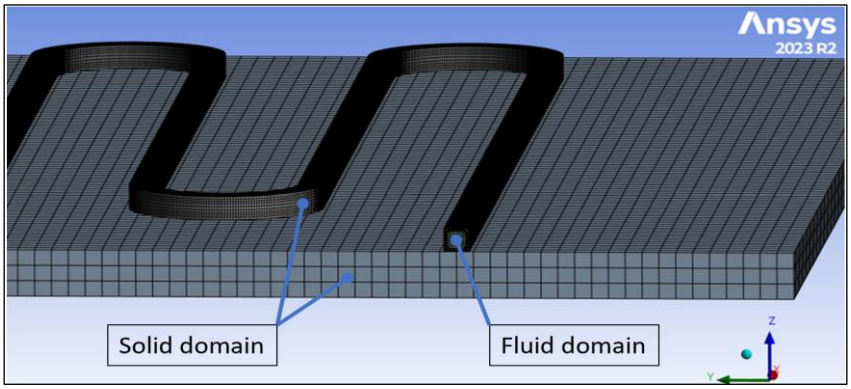

Fig. 2. Mesh generation.

Mesh Independence Test

The mesh independence test was conducted by evaluating six different meshing sizes. The mesh was tested by applying 0.10 m, 0.15 m, 0.20 m, 0.25 m, 0.30 m, and 0.35 m of elements to the mesh size for the grid independence test (GIT) to ensure that the grid is suitable for achieving a stable and converged solution. Pure water was used to determine the cell temperature for the mesh independence study, as shown in Fig 3. The grid size of 0.15 m provided a stable cell temperature, with variations not exceeding 0.05%. Thus, a meshing size of 0.15 m with elements of 1.427 million was considered the best mesh quality for further analysis.

Boundary Conditions

The boundary conditions and domains applied follow the research of Karaaslan & Menlik (2021). The flow of working fluids at different inlet velocities was simulated using a velocity inlet boundary condition at the inlet. In this way, different flow rates can be evaluated on the same type of fluid. A pressure outlet boundary condition was used at the outlet, considering that the flow field was incompressible with a known

https://doi.org/10.24191/jmeche.v22i3.5754

static pressure. Such a setup allows the flow development to remain stable throughout the computational domain and provides an accurate assessment of thermal and hydraulic performance. Solar radiation was simulated as heat flux applied to the exterior of the solar cells, based on the values provided (Karaaslan & Menlik, 2021). Table 2 summarizes the implemented boundary conditions for the simulation.

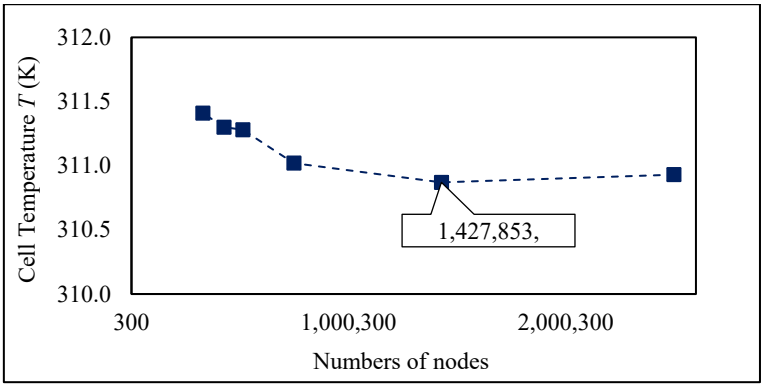

Fig. 3. Grid independence test.

Table 2. Summary of boundary conditions (Karaaslan & Menlik, 2021)

Boundary properties	Value	Unit
Heat flux as solar radiation	1000	W/m^2
Inlet velocity	0.0272 – 0.1360	m/s
Inlet temperature	303	K
Inlet pressure	0	Pa
Outlet pressure	1	Pa

Thermophysical Properties

The thermophysical properties of water and Al_2O_3:SiO_2 hybrid nanofluids are taken from the published work of Khalid et al. (2021) as listed in Table 3.

Table 3. Thermophysical properties of studied working fluids (Khalid et al., 2021; Yatim et al., 2021)

Fluid name	Thermal conductivity, K (W/mK)	Specific heat, Cp (J/kgK)	Viscosity (kg/ms)	Density (kg/m^3)
Al_2O_3	36	765	-	4000
SiO_2	1.4	745	-	2220
Water	0.6194	4070	0.000773	995.2

To accurately study the electrical and thermal performance of the Al_2O_3:SiO_2 hybrid nanofluids in cooling applications for solar PVT panels, it is necessary to calculate their density and specific heat to simulate ANSYS Fluent. Thus, the properties of hybrid nanofluids were calculated using the correlation as presented in Figure 4.

Solver Settings and Governing Equations

The solver used is a laminar model as the calculated Reynolds number is within the range of the laminar flow (Re < 2300). The energy equation is enabled to evaluate the heat transfer between fluid and solid domains. This simulation uses a pressure-based and steady-state solver, which is more efficient in terms of

https://doi.org/10.24191/jmeche.v22i3.5754

computational time than a transient simulation. The pressure-velocity coupling solution is handled with the Coupled Method. In discretization, a gradient is treated with the least squares method on cell bases, while pressure is discretized in second order. Both momentum and energy equations are uniformly discretized using a second-order upwind scheme. Convergence criteria have been set at a default residual tolerance of 0.001 for perpetuity as well as velocities in x, y, and z directions, and energy in ANSYS Fluent. A hybrid initialization method is used, whereby 1000 iterations are performed to ensure accuracy and convergence of the results accessed. Numerical solutions deal with the governing formula for mass balance, momentum balance, and energy conservation, but also include how the solid interacts with the fluid, as in Table 5.

Certain assumptions have been introduced to streamline the simulation analysis process (Karaaslan & Menlik, 2021).

(i) The base fluid and nanoparticles are simulated as a single phase, and it is in thermally equilibrium.
(ii) The thermo-physical characteristics of materials utilized in PV/T layers remain unaffected by temperature variations.
(iii) The working fluids are maintained at a constant density, with a uniform, laminar flow that is fully developed at the outlet.
(iv) The side surfaces of the components, the outer surface of the pipe, and the lower surface of the absorber plate are maintained in adiabatic conditions.

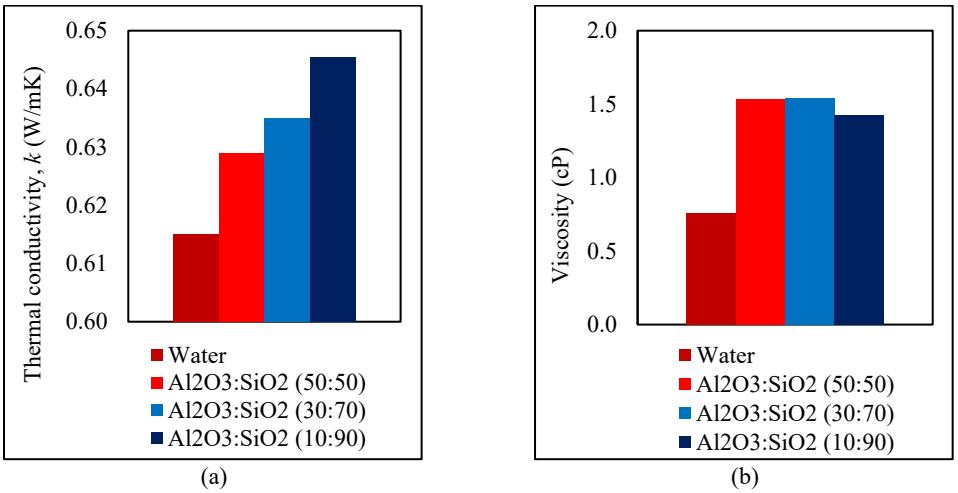

Fig. 4. Thermophysical properties of working fluids for (a) thermal conductivity at different fluids (Khalid et al., 2021) and (b) viscosity at different fluids (Khalid et al., 2021).

Table 4. Correlations in determining thermophysical properties of alumina-silica hybrid nanofluids (Karaaslan & Menlik, 2021)

Property	Hybrid nanofluid
Density, ρ_{hnf}	$\rho_{hnf} = \varphi_{p1}\rho_{p1} + \varphi_{p2}\rho_{p2} + (1 - (\varphi_{p1} + \varphi_{p2}))\rho_{bf}$
Specific heat, C_{hnf}	$(\rho C)_{hnf} = \varphi_{p1}\rho_{p1}C_{p1} + \varphi_{p2}\rho_{p2}C_{p2} + (1 - (\varphi_{p1} + \varphi_{p2}))C_{bf}$

Energy Analysis

System efficiency is determined by the energy input and the work performed within the system. Thermal efficiency in a solar *PV/T*, η_{th} refers to the proportion of absorbed solar energy that is converted into useful heat, considering factors like conduction, convection, and radiation losses. Meanwhile, the electrical efficiency of a solar *PV/T*, η_{elec} represents the ratio of electrical power output to the incident solar radiation, influenced by factors like temperature, material properties, and system design.

https://doi.org/10.24191/jmeche.v22i3.5754

Table 5. Correlations governing equation used in solver settings (Ali et al., 2023)

Numerical solution	Governing equation
Continuity equation	$\frac{\partial u}{\partial x}+\frac{\partial v}{\partial y}=0$
Momentum equation	$u\frac{\partial u}{\partial x}+v\frac{\partial v}{\partial y}=U\frac{\partial u}{\partial x}+\frac{\mu_{nf}}{\rho_{nf}}\frac{\partial^2 u}{\partial y^2}$
Energy equation	$u\frac{\partial T}{\partial x}+v\frac{\partial T}{\partial y}=\frac{k_{nf}}{(\rho Cp)_{nf}}\frac{\partial^2 T}{\partial y^2}+Q*(T-T_\infty)+\frac{\mu_{nf}}{(\rho Cp)_{nf}}\left(\frac{\partial u}{\partial y}\right)^2$

As hybrid systems, PV/T configurations integrate both electrical and thermal efficiency, allowing their combined effect to be considered in total efficiency calculations. The efficiency Equations 1 to 3 are retrieved from Hissouf et al. (2020).

$$\eta_T = \eta_{th} + \eta_{ele} \tag{1}$$

$$\eta_{th} = \frac{\dot{m}C_p(T_{out} - T_{in})}{GA} \tag{2}$$

$$\eta_{ele} = \eta_r\left[\left(1 - \beta_r(T_{cell} - T_r)\right)\right] \tag{3}$$

where G represents the solar radiation, η_r represent the solar cells efficiency at the reference temperature T_r and β_r (value of the temperature coefficient) represents the PV cell temperature coefficient.

Heat Transfer Analysis

Heat transfer analysis involves the heat transfer coefficient and the Nusselt number, Nu number (Johari et al., 2022; Yatim et al., 2021) and represented by Equations 4 to 5.

$$h = \frac{q}{T_p - \left(\frac{T_i + T_o}{2}\right)} \tag{4}$$

where h represent the heat transfer coefficient, q represents the heat flux, T_p represent the average plate temperature, T_i represent the inlet temperature and T_o represent the outlet temperature of the cooling tube. Where Nu represent the Nusselt number, D_i represent the inlet diameter and k represent thermal conductivity. Meanwhile, the additional pumping power required to circulate the cooling fluids is used Equation 6. Where Q represent the calculated volume flow rate, and Δp is the pressure drop difference.

$$Nu = \frac{hD_i}{k} \tag{5}$$

$$\mathrm{W}_{pump} = \dot{Q} \times \Delta p \tag{6}$$

RESULTS AND DISCUSSION

Validation of the Simulation Study

The simulation was validated against existing literature data (Karaaslan & Menlik, 2021) using a base fluid of water to ensure accuracy before assessing the hybrid nanofluids' heat transfer analysis. As scrutinized in Fig 5, the cell temperature trend indicates that the discrepancy between the base fluid and

https://doi.org/10.24191/jmeche.v22i3.5754

literature data decreases with increasing velocity and stabilizes at higher velocities. The simulation statistic exhibits a sufficient accuracy value, ranging from 2.24% to 4.62% deviation from the literature review. The deviation of the simulation data might be due to the differences in velocities used. The velocities that are used in the simulation are based on the cross-sectional area of the cooling tube.

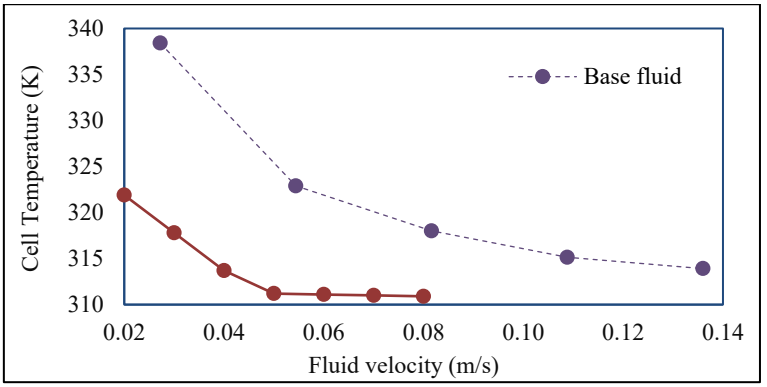

Fig. 5. Base data validation.

Temperature Effect

The simulation operates under constant heat flow and inlet fluid temperature conditions. Therefore, its efficiency is mainly influenced by variations in the inlet fluid velocity as well as the output temperature. Fig 6 depicts the reduction of average cell temperature for thermal analysis. The cell temperature drops with increasing fluid velocity for all working fluids. The observed cooling effect shows that water has the highest cell temperature as compared to other Al_2O_3:SiO_2 hybrid nanofluids. The Al_2O_3:SiO_2 hybrid nanofluid with a ratio of (10:90) shows a significant improvement in the reduction of cell temperature in comparison to the base fluid of water, with a 2.57% improvement. This outcome is expected as all volume ratios of hybrid nanofluids have a higher thermal conductivity than water. The simulation findings were consistent with the research conducted by Khalid et al. (2021) as the study revealed that Al_2O_3:SiO_2 hybrid nanofluids of a 10:90 ratio have higher thermal conductivity, followed by 30:70 and 50:50.

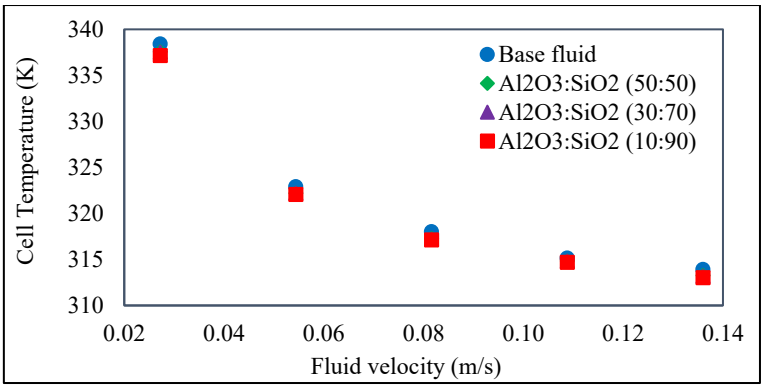

Fig. 6. Cell temperature at different velocities.

As observed in Fig 5, at 0.0272 m/s, the plate temperatures are 338.41 K, 337.57 K, 337.52 K, and 337.16 K for water, Al_2O_3:SiO_2 (50:50), Al_2O_3:SiO_2 (30:70), and Al_2O_3:SiO_2 (10:90), respectively. As the

https://doi.org/10.24191/jmeche.v22i3.5754

velocity increases to 0.0816 m/s, these temperatures decrease to 318.01 K, 317.28 K, 317.22 K, and 317.13 K, respectively. This trend indicates that the heat transfer rate from the plate to the cooling fluid is improved at higher fluid velocities, as it lowers the cell temperatures, as studied in Karaaslan & Menlik (2021).

Fig 7 represents the temperature distribution to examine the reduction in PVT panel temperature with different cooling fluids at an inlet fluid velocity of 0.0816 m/s. The outcome shows that the flow in the cooling tube is incapable of cooling the PVT panel uniformly. A colder working fluid entering the serpentine tube gets warmer as it absorbs the heat, making the temperature difference between the cooling fluid and the panel smaller. This has resulted in hot temperatures at the other end of the PVT panel, as shown in Fig 7. In Fig 7(a), water shows a prominent, larger red spot, as compared to the others, reflecting its limited heat transfer capability. The temperature distribution shows a progressive reduction in red spots, indicating a better panel temperature in 10:90 Al_2O_3:SiO_2 hybrid nanofluids. The dark blue region showing the coldest temperature also increases as the red spot decreases. The slight differences in temperature reduction among the 30:70 and 50:50 mixture ratios of nanofluids are due to the low volume concentration of 0.5% used for hybrid nanofluids. Sardarabadi & Passandideh-Fard (2016) studies indicate that the cooling efficiency increases with higher volume concentrations.

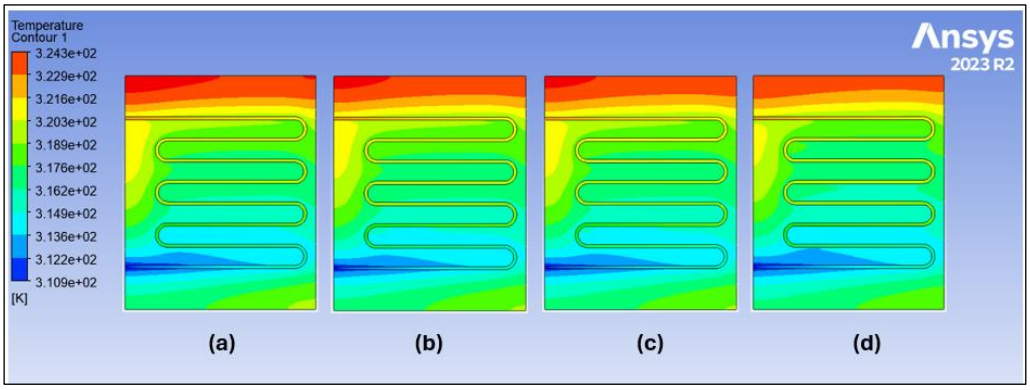

Fig.7. Temperature distribution at PV panel of (a) water (b) 50:50 (c) 30:70 (d) 10:90.

As shown in Fig 8, the outlet temperature of the working fluids decreases with increasing inlet velocity. This trend is attributed to the reduced residence time of the fluid within the cooling channel at higher velocities, resulting in less heat absorption. At an inlet velocity of 0.0272 m/s, the average outlet temperatures recorded were 342.41 K for water, 342.49 K for Al_2O_3:SiO_2 (50:50), 342.60 K for Al_2O_3:SiO_2 (30:70), and 342.81 K for Al_2O_3:SiO_2 (10:90). At a higher inlet velocity of 0.0816 m/s, the corresponding outlet temperatures were 317.14 K, 317.20 K, 317.17 K, and 317.59 K, respectively. Although the differences among the outlet temperatures are relatively small, hybrid nanofluids consistently exhibit slightly higher outlet temperatures compared to the base fluid. This is attributed to their enhanced thermal conductivity, which allows for greater heat absorption and more effective reduction of the cell temperature, as supported by Hissouf et al. (2020).

Fig 9 represents the temperature distribution of outlet temperature at the tube cross-section for water, Al_2O_3:SiO_2 (50:50), Al_2O_3:SiO_2 (30:70), and Al_2O_3:SiO_2 (10:90) hybrid nanofluid at 0.0816 m/s inlet fluid velocity, respectively. This outcome is connected to the fact that hybrid nanofluids have higher thermal conductivity as compared to water, which absorbs heat more efficiently from the solar PVT panel. It can be observed that the red spot in Fig 9(d) is more prominent due to its greater thermal conductivity as opposed to other compositions and water. As discussed in Fig 6, Al_2O_3:SiO_2 (10:90) hybrid nanofluids exhibit the lowest cell temperature, as they absorb more heat from the system effectively. As a result, more heat is carried away from the heated regions, leading to a higher outlet temperature.

https://doi.org/10.24191/jmeche.v22i3.5754

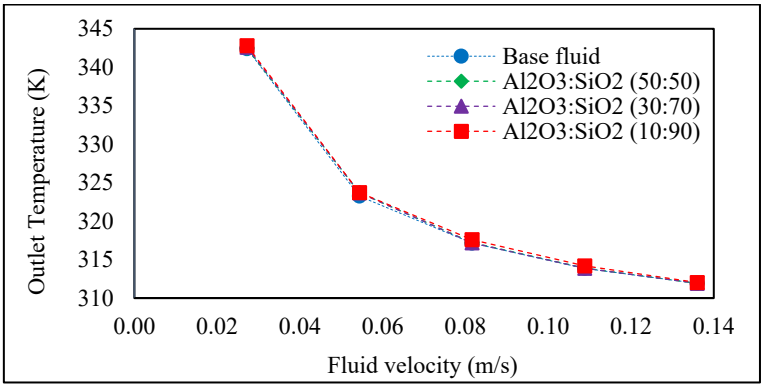

Fig. 8. Outlet temperature at different velocities.

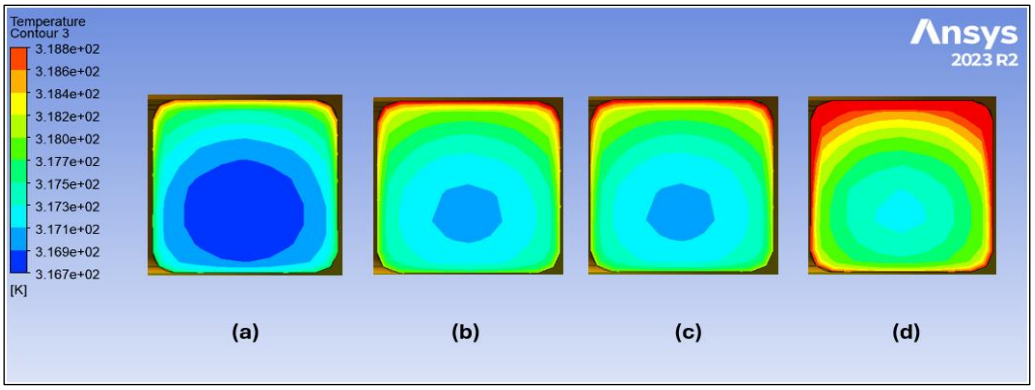

Fig. 9. Temperature distribution at tube construction of (a) water, (b) 50:50, (c) 30:70, and (d) 10:90.

Heat Transfer Coefficient

The influence of different cooling fluids on the heat transfer coefficient was further investigated. Fig 10 illustrates the heat transfer coefficients of all working fluids at various flow velocities. Among them, the Al_2O_3:SiO_2 (10:90) hybrid nanofluid exhibited the highest enhancement, with a 16.95% increase compared to the base fluid. This improvement is attributed to the superior thermal conductivity of the Al_2O_3:SiO_2 (10:90) nanofluid, which enhances its heat transfer capability. These results are consistent with the findings reported by Yatim et al. (2021) further confirming that the Al_2O_3:SiO_2 (10:90) hybrid nanofluid offers improved thermal management performance compared to other mixture ratios and the base fluid. The random movement of nanoparticles due to Brownian motion enhances thermal conductivity and fluid mixing in nanofluids, leading to a higher heat transfer coefficient by improving energy dispersion and reducing thermal resistance (Hamzan et al., 2025).

Nusselt Number

Fig 11 presents the Nusselt number, derived from the calculated heat transfer coefficients. As expected, the Nusselt number increases linearly with rising fluid velocity. Furthermore, hybrid nanofluids consistently exhibit higher Nusselt numbers than the base fluid (water). Among the tested mixtures, the Al_2O_3:SiO_2 (10:90) hybrid nanofluid demonstrated the highest performance, achieving a maximum enhancement of 12.06% over water at a velocity of 0.1360 m/s. In contrast, the Al_2O_3:SiO_2 (30:70) mixture showed the lowest improvement, with a modest increase of 0.22% at 0.0544 m/s. These variations in performance are

https://doi.org/10.24191/jmeche.v22i3.5754

primarily attributed to differences in thermal conductivity and convective heat transfer characteristics among the various nanofluid compositions.

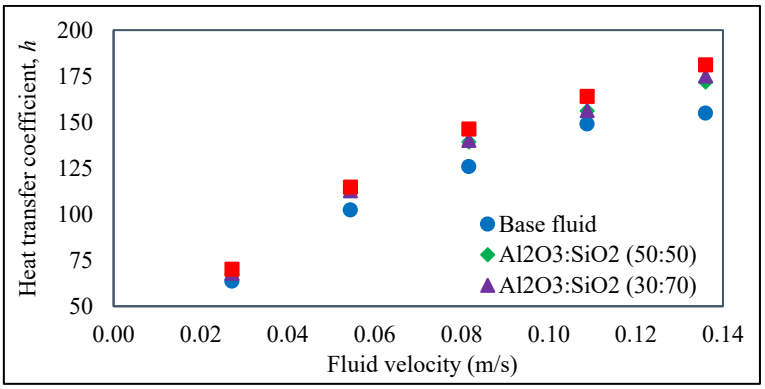

Fig. 10. Heat transfer coefficient at different velocities.

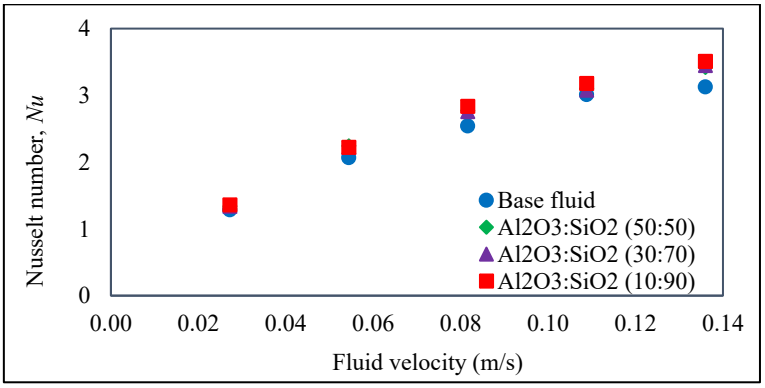

Fig. 11. Nusselt number at different velocities.

Pressure Drop

Pressure drops occur as a consequence of the viscous forces of working fluids in the tube surface. The increase in viscosity resulted in a rise in pressure losses, which requires more pump power. Therefore, high viscosity is a drawback for the thermal performance of hybrid nanofluids.

Fig 12 shows the pressure difference between the inlet and outlet fluids inside the serpentine tube studied. The highest pressure drop was observed at the Al_2O_3:SiO_2 (30:70) hybrid nanofluids, which reached up to 387.91 Pa at a speed of 0.1360 m/s. This is significantly higher than the base fluid's pressure drops of 286.34 Pa. The base fluid provided the lowest pressure drop across all speeds as it had the lowest viscosity value. Hybrid nanofluids have a larger pressure drop due to their higher density and viscosity. Thus, the hybrid nanofluids (30:70) exhibit the greatest pressure drop when compared to (50:50) and (10:90), due to their highest viscosity values. Thus, Al_2O_3:SiO_2 30:70 hybrid nanofluid has the most friction losses as compared to other mixture ratios of hybrid nanofluids and base fluid. This result is well aligned with the conclusions made by the findings of Yatim et al. (2021) and Karaaslan & Menlik (2021) where higher viscosity hybrid nanofluids experience greater pressure drops due to increased friction losses compared to base fluids.

https://doi.org/10.24191/jmeche.v22i3.5754

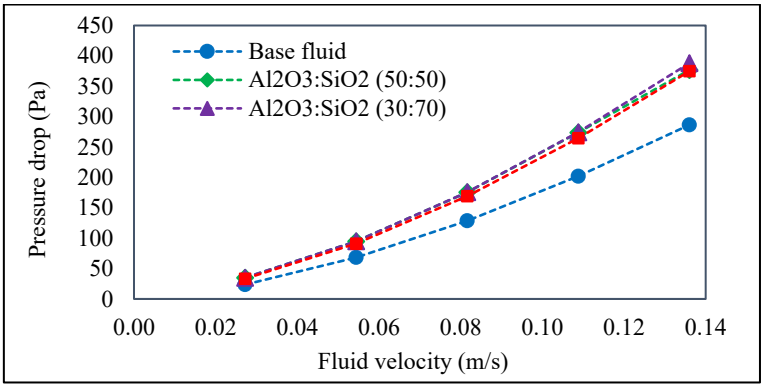

Fig. 12. Pressure drops at different inlet velocities.

Pumping Power

The pumping power is then evaluated from the pressure drop readings on the influence of hybrid nanofluids on the additional pumping power required to cool the panel. Fig 13 shows the required pumping power for all the working fluids. Al_2O_3:SiO_2 (10:90) hybrid nanofluids exhibited greater required pumping energy than water, reaching 0.0063 W at a maximum velocity of 0.1360 m/s, similar to the 50:50 and 30:70 nanofluids. All fluids have a relatively low pumping power needed at lower velocities, starting around 0.0001 W. It is observed that the amount of pumping power increases with the increasing fluid velocity. At a speed of 0.0816 m/s, the pumping working power for the Al_2O_3:SiO_2 (10:90) nanofluid is 0.0017 W, slightly less than 50:50 and 30:70 hybrid nanofluids, which require 0.0018 W. At higher velocities, the nanofluid with a ratio of Al_2O_3:SiO_2 (10:90) consistently requires less pumping power than other ratios. This suggests that the lower viscosity of Al_2O_3:SiO_2 (10:90) hybrid nanofluid helps minimize flow resistance. However, despite requiring higher pumping power than water, it demonstrates a balanced performance with moderate increases in pumping power compared to the 50:50 and 30:70 ratios. The hybrid nanofluids Al_2O_3:SiO_2 (10:90) ratio may offer a feasible compromise between enhanced thermal performance and manageable pumping power requirements. A greater amount of pumping power is less practical as it increases parasitic loss.

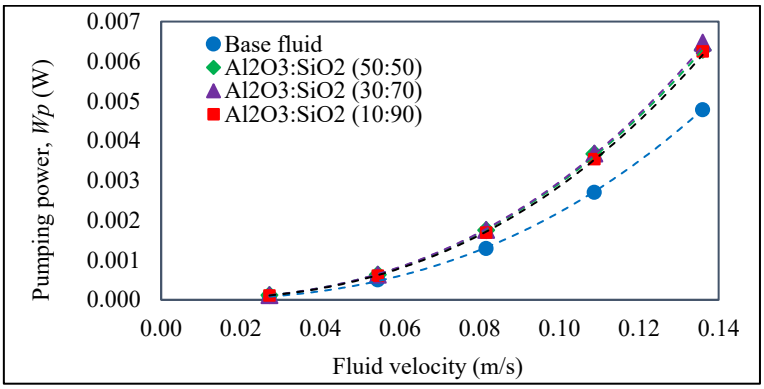

Fig. 13. Pumping power at different velocities.

https://doi.org/10.24191/jmeche.v22i3.5754

Thermal Efficiency

Fig 14 shows that the thermal performance of Al_2O_3:SiO_2 hybrid nanofluids is more favourable than the base fluid of water. Observation shows that the thermal efficiency of the Al_2O_3:SiO_2 (10:90) hybrid nanofluids is the highest among all fluids studied, followed by 50:50 and 30:70. Meanwhile, the base fluid shows the lowest thermal efficiency. Using Al_2O_3:SiO_2 (10:90) hybrid nanofluid provides a maximum increment of 4.75% at 0.0816 m/s compared to water, demonstrating significantly enhanced heat transfer capabilities and cooling performance. This is due to the increase in the Brownian motion of nanoparticles in hybrid nanofluids, which resulted in an improved heat transfer (Johari et al., 2022).

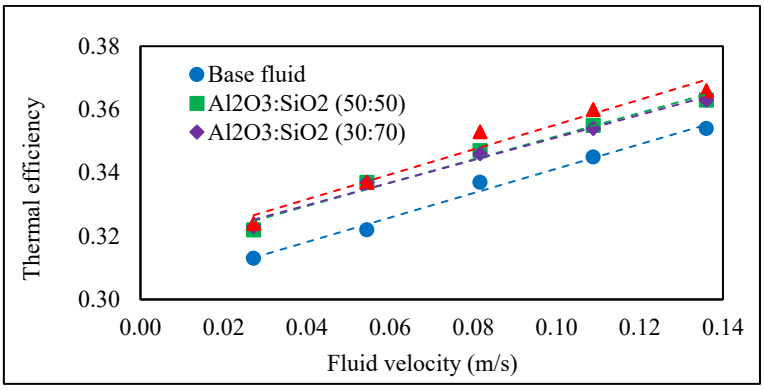

Fig. 14. Thermal efficiency at different inlet velocities.

Electrical Efficiency

Fig 15 shows that adding Al_2O_3:SiO_2 hybrid nanofluid into the water positively affects the electrical efficiency rather than using water alone as the cooling medium. The Al_2O_3:SiO_2 (10:90) hybrid nanofluid provides the highest electrical efficiencies. At the lowest speed of 0.0272 m/s, the electrical efficiency of water is 0.141, whereas the Al_2O_3:SiO_2 (50:50) and Al_2O_3:SiO_2 (30:70) hybrid nanofluids show a slight increase to 0.142, resulting in an increment of 0.71%. The Al_2O_3:SiO_2 (10:90) hybrid nanofluid provides a more significant increment of 1.42%, reaching an electrical efficiency of 0.143. For speeds of 0.1088 m/s and 0.1360 m/s, the electrical efficiencies of water are 0.159 and 0.160, respectively. The increments for (50:50) and (30:70) nanofluids are consistent at 0.63%, reaching efficiencies of 0.161. The (10:90) nanofluid shows an increment of 0.63% with an efficiency of 0.161. For electrical efficiency, the Al_2O_3:SiO_2 (10:90) consistently delivers the highest increment in electrical efficiency compared to water, with maximum increments of up to 1.42% at lower speeds and maintaining a consistent improvement at higher speeds. This is attributable to the colder panel temperature due to the higher value of thermal conductivity of hybrid nanofluids than water.

Fig 16 shows the total efficiency of all working fluids at different inlet velocities. It shows that the rise in inlet velocity of the working fluid positively affects the overall efficiency of the energy analysis. At 0.0272 m/s, the total efficiency values are 0.454, 0.464, 0.465, and 0.467 for water, Al_2O_3:SiO_2 (50:50), Al_2O_3:SiO_2 (30:70), and Al_2O_3:SiO_2 (10:90), respectively. These values improve to 0.494, 0.504, 0.504, and 0.511 at 0.0816 m/s inlet fluid velocity. The increased trends in efficiency are consistent with other research in the literature, as Hissouf et al. (2020) shows that higher inlet fluid velocities improve the cooling effect on the panel, thus improving the overall performance of the system. These highlight the superior thermal and electrical performance of nanofluids compared to water at higher velocities.

https://doi.org/10.24191/jmeche.v22i3.5754

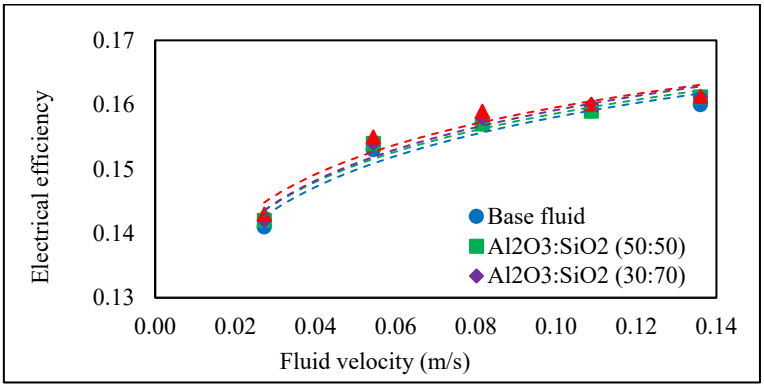

Fig. 15. Electrical efficiency at different inlet velocities.

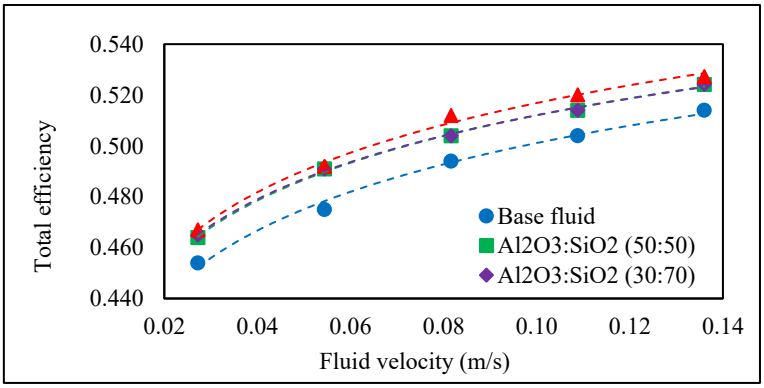

Fig. 16. Total efficiency at different inlet velocities.

CONCLUSION

In this present study, the impact of using water and Al_2O_3:SiO_2/Water hybrid nanofluids as coolant on the thermal management of a solar PVT panel was evaluated through numerical simulations. In this study, CFD simulations were conducted under various operating conditions to evaluate the performance of three different hybrid nanofluid mixture ratios at varying fluid flow velocities. The results demonstrated that all hybrid nanofluid combinations exhibited superior cooling performance compared to the base fluid (water), which is demonstrated by the increase in heat transfer coefficients and Nusselt numbers. Among the studied mixture ratios, the Al_2O_3:SiO_2 (10:90) hybrid nanofluid showed the most notable temperature reduction in solar PVT panels, leading to an improvement in thermal efficiency of up to 4.75% and an approximate 1.42% enhancement in electrical efficiency relative to water. The 10:90 hybrid nanofluid also shows the highest heat absorption, with 16.95% increments in the heat transfer coefficient. Pumping capacity increases for hybrid nanofluids as they undergo a greater pressure drop in the cooling tube. The Al_2O_3:SiO_2/Water hybrid nanofluids in a mixture ratio of 10:90 exhibit the lowest pressure drop among other ratios, confirming their feasibility as an alternative cooling medium. Overall, the 10:90 hybrid Al_2O_3:SiO_2 nanofluids show the most feasible ratio as they exhibited the most cell temperature reduction, which gives the highest thermal and electrical efficiency for cooling of a solar PVT panel.

https://doi.org/10.24191/jmeche.v22i3.5754

ACKNOWLEDGEMENTS/ FUNDING

The authors would like to acknowledge Universiti Teknologi MARA under the Geran Insentif Penyeliaan Scheme: Grant No. 600-RMC/GIP 5/3 (009/2024) and the Faculty of Mechanical Engineering for the research funding and technical assistance provided.

CONFLICT OF INTEREST STATEMENT

The authors agree that this research was conducted in the absence of any self-benefits, commercial or financial conflicts and declare the absence of conflicting interests with the funders.

AUTHORS' CONTRIBUTIONS

The authors confirm their contribution to the paper as follows: **study conception and design**: Irnie Azlin Zakaria, Nor Afifah Yahaya; **data collection**: Nur Hanani Radzuan; **analysis and interpretation of results**: Nur Hanani Radzuan, Irnie Azlin Zakaria, Anwar Ilmar Ramadhan; **draft manuscript preparation**: Nur Hanani Radzuan; **Supervision**: Irnie Azlin Zakaria.

REFERENCES

Akrouch, M. A., Chahine, K., Faraj, J., Hachem, F., Castelain, C., & Khaled, M. (2025). Advancements in cooling techniques for enhanced efficiency of solar photovoltaic panels: A detailed comprehensive review and innovative classification. Energy and Built Environment, 6(2), 248-276.

Ali, A., Alhussein, M., Aurangzeb, K., & Akbar, F. (2023). The numerical analysis of Al2O3Cu/water hybrid nanofluid flow inside the serpentine absorber channel of a PVT; the overall efficiency intelligent forecasting. Engineering Analysis with Boundary Elements, 157, 82-91.

Alqatamin, A., & Jinzhan, S. (2025). Numerical analysis and design of photovoltaic-thermal (PVT) system with novel water-cooling channel structure integrated with perforated v-shape fins. Renewable Energy, 243, 122587.

Awais, M., Ullah, N., Ahmad, J., Sikandar, F., Ehsan, M. M., Salehin, S., & Bhuiyan, A. A. (2021). Heat transfer and pressure drop performance of nanofluid: A state-of- the-art review. International Journal of Thermofluids, 9, 100065.

Hamzan, N., Zakaria, I. A., Ghani, J. A., Halim, N. H. A., Azmi, W. H., Solihin, Z. H., & Ahmad, A. A. (2025). The SiO2:TiO2 hybrid biodegradable nanolubricant for sustainable machining: The stability, thermo-physical and tribology perspectives. Tribology International, 207, 110614.

Hamzat, A. K., Sahin, A. Z., Omisanya, M. I., & Alhems, L. M. (2021). Advances in PV and PVT cooling technologies: A review. Sustainable Energy Technologies and Assessments, 47, 101360.

Hissouf, M., Feddaoui, M., Najim, M., & Charef, A. (2020). Numerical study of a covered Photovoltaic-Thermal Collector (PVT) enhancement using nanofluids. Solar Energy, 199, 115-127.

Hussien, A., Eltayesh, A., & El-Batsh, H. M. (2023). Experimental and numerical investigation for PV cooling by forced convection. Alexandria Engineering Journal, 64, 427-440.

https://doi.org/10.24191/jmeche.v22i3.5754

Johari, M. N. I., Zakaria, I. A., & Affendy, N. S. M. (2022). Thermal behaviour of hybrid nanofluids in water: Bio glycol mixture in cooling plates of PEMFC. CFD Letters, 14(6), 43-55.

Johari, M. N. I., Zakaria, I. A., Azmi, W. H., & Mohamed, W. A. N. W. (2022). Green bio glycol Al2O3-SiO2 hybrid nanofluids for PEMFC: The thermal-electrical-hydraulic perspectives. International Communications in Heat and Mass Transfer, 131, 105870.

Karaaslan, I., & Menlik, T. (2021). Numerical study of a photovoltaic thermal (PV/T) system using mono and hybrid nanofluid. Solar Energy, 224, 1260-1270.

Kazemian, A., Salari, A., Ma, T., & Lu, H. (2022). Application of hybrid nanofluids in a novel combined photovoltaic/thermal and solar collector system. Solar Energy, 239, 102-116.

Khalid, S., Zakaria, I. A., Azmi, W. H., Johari, M. N. I., & Mohamed, W. A. N. W. (2024). Improving heat transfer through alumina-silica nanoparticles suspension: An experimental study on a single cooling plate. Experimental Heat Transfer, 38(4), 307–327.

Khalid, S., Zakaria, I., Azmi, W. H., & Mohamed, W. A. N. W. (2021). Thermal–electrical–hydraulic properties of Al2O3–SiO2 hybrid nanofluids for advanced PEM fuel cell thermal management. Journal of Thermal Analysis and Calorimetry, 143(2), 1555-1567.

Khalid, S., Zakaria, I. A., & Mohamed, W. A. N. W. (2019). Comparative analysis of thermophysical properties of Al2O3 and SiO2 nanofluids. Journal of Mechanical Engineering, 8(1), 153-163.

Nabi, H., Gholinia, M., Khiadani, M., & Shafieian, A. (2023). Performance enhancement of photovoltaic-thermal modules using a new environmentally friendly paraffin wax and red wine-rGO/H2O Nanofluid. Energies, 16(11), 4332.

Praveenkumar, S., Agyekum, E. B., Kumar, A., & Velkin, V. I. (2023). Thermo-enviro-economic analysis of solar photovoltaic/thermal system incorporated with u-shaped grid copper pipe, thermal electric generators and nanofluids: An experimental investigation. Journal of Energy Storage, 60, 106611.

Preeti & Ojjela, O. (2022). Numerical investigation of heat transport in alumina–silica hybrid nanofluid flow with modeling and simulation. Mathematics and Computers in Simulation, 193, 100-122.

Price, Ben. (2025). Solar panel sizes & dimensions UK (Do they even matter). Solar advice. https://heatable.co.uk/solar/advice/solar-panel-sizes

Rostami, M. N., Dinarvand, S., & Pop, I. (2018). Dual solutions for mixed convective stagnation-point flow of an aqueous silica–alumina hybrid nanofluid. Chinese Journal of Physics, 56(5), 2465-2478.

Salehi, R., Jahanbakhshi, A., Ooi, J. B., Rohani, A., & Golzarian, M. R. (2023). Study on the performance of solar cells cooled with heatsink and nanofluid added with aluminum nanoparticle. International Journal of Thermofluids, 20, 100445.

Sardarabadi, M., & Passandideh-Fard, M. (2016). Experimental and numerical study of metal-oxides/water nanofluids as coolant in photovoltaic thermal systems (PVT). Solar Energy Materials and Solar Cells, 157, 533-542.

Vahidinia, F., Khorasanizadeh, H., & Aghaei, A. (2021). Comparative energy, exergy and CO2 emission evaluations of a LS-2 parabolic trough solar collector using Al2O3/SiO2-Syltherm 800 hybrid nanofluid. Energy Conversion and Management, 245, 114596.

Yatim, M. S. M., Zakaria, I. A., Roslan, M. F., Mohamed, W. A. N. W., & Mohamad, M. F. (2021). Heat transfer and pressure drop characteristics of hybrid Al2O3-SiO2. Journal of Mechanical Engineering, 18(2), 145-159.

https://doi.org/10.24191/jmeche.v22i3.5754

Hussien, A., Eltayesh, A., & El-Batsh, H. M. (2023). Experimental and numerical investigation for PV cooling by forced convection. *Alexandria Engineering Journal*, *64*, 427–440. https://doi.org/10.1016/j.aej.2022.09.006

Khalid, S., Zakaria, A., Najmi, W. A., Mohamed, W., Azmi, W., & Hamzah, W. (2019). Comparative analysis of thermophysical properties of Al 2 O 3 and SiO 2 nanofluids. *Journal of Mechanical Engineering*, *8*(1), 153–163.

Praveenkumar, S., Agyekum, E. B., Kumar, A., & Velkin, V. I. (2023). Thermo-enviro-economic analysis of solar photovoltaic/thermal system incorporated with u-shaped grid copper pipe, thermal electric generators and nanofluids: An experimental investigation. *Journal of Energy Storage*, *60*. https://doi.org/10.1016/j.est.2023.106611

Zakaria, I. A., Ahmad Najmi Wan Mohamed, W., Mohd Ihsan Mamat, A., Imran Sainan, K., Rozi Mat Nawi, M., & Hassan Najafi, G. (2018). Numerical Analysis Of Al 2 O 3 Nanofluids In Serpentine Cooling Plate Of PEM Fuel Cell. *Journal of Mechanical Engineering*, *5*(1), 1–13.

Zakaria, I. A., Michael, Z., Hanapi, S., & Mohamed, W. A. N. W. (2014). Thermal and Electrical Experimental Characterization of Ethylene Glycol and Water Mixture Coolants for a 400 W Proton Exchange Membrane Fuel. *Applied Mechanics and Materials (Volume 660)*, 391–396.

https://doi.org/10.24191/jmeche.v22i3.5754